Published in "Europhysics Letters 96(2): 26002, 2011"
which should be cited to refer to this work.

Phonon generation in condensed ^{4}He by laser-excited atomic bubbles

P. Moroshkin[(a)], V. Lebedev and A. Weis

Department of Physics, University of Fribourg - Chemin du Musée 3, 1700 Fribourg, Switzerland

Abstract – We discuss the interaction between nanometer-sized defects (atomic bubbles) and elementary excitations (phonons) in quantum fluids and solids. We observe that optical excitations in embedded metal atoms induce bubble expansions/contractions that create strongly localized phonon wave packets in the quantum matrix. We derive the structure and dynamics of these vibronic excitations from the experimental laser-induced fluorescence spectra of Au and Cu atoms in liquid and solid He. The atomic vibrations are found to be strongly damped on the 50 Å and 5 ps scales in agreement with pure hydrodynamic estimations.

The dynamics of quantum fluids and solids is described in terms of quantized elementary excitations (such as, *e.g.*, phonons and rotons in HeII [1]) with energies E and momenta k of meV range (tens of K) and a few Å^{-1}, respectively. The most widely used method for probing these excitations is the inelastic scattering of neutrons having comparable energies and momenta. Each scattering event creates one phonon (roton), whose parameters E and k can be determined from the energy and momentum of the scattered neutron. First neutron scattering experiments on superfluid helium were reported in the 1950s, and nowadays the technique is still widely used, in particular in connection with excitations in thin helium films [2], helium confined in nanoporous media [3], and possible manifestations of supersolidity [4]. Scattering experiments can also be performed with optical photons [5] ($E \simeq 2.5\,\text{eV}$, $k \simeq 10^{-4}\,\text{Å}^{-1}$). However, the smallness of the photon momentum implies that only $k \approx 0$ optical phonons (which exist only in solids) or pairs of counterpropagating excitations can be created.

Impurity atoms and molecules represent another class of nanoscopic objects that may create elementary excitations in condensed helium [6–10]. However, their potential for probing the dynamics of quantum fluids and solids at the microscopic level has not been exploited in depth so far. The main advantage of atomic dopants over other probes is that they can be interrogated by means of laser radiation. Therefore, a variety of laser-spectroscopic and time-resolved methods can be applied for obtaining information on the matrix excitations. The mechanism of impurity-phonon interactions at the microscopic scale is not quantitatively understood at present. In particular, it is not clear how the presence of dopants modifies the spectrum and dispersion relation of the excitations in the helium sample, *e.g.*, via the appearance of localized modes which do not exist in pure condensed helium.

Here we present a simple hydrodynamic model for describing the dynamics of a vibrating atomic bubble. Our analysis reveals two regimes of the impurity-phonon interaction which we shall refer to as *quasiclassical* and *quantum*. We analyze existing optical data of impurity atoms in condensed helium and present a new laser-spectroscopic study of condensed ^{4}He doped with the transition-metal atoms Au and Cu. Our results demonstrate that in the quantum regime their laser-induced fluorescence spectra yield complete information on the structure and dynamics of the phonon wave packet generated by the atomic-bubble motion.

The structure of the defects formed by metal atoms embedded in liquid and solid helium has been studied since the 1980s (reviewed in [11]). The valence electron of the metal atom strongly repels the closed-shell He atoms due to the Pauli principle. The dopant thus forms a nanometer-sized cavity, of radius R_b, called "atomic bubble". Due to

[(a)] E-mail: peter.moroshkin@unifr.ch

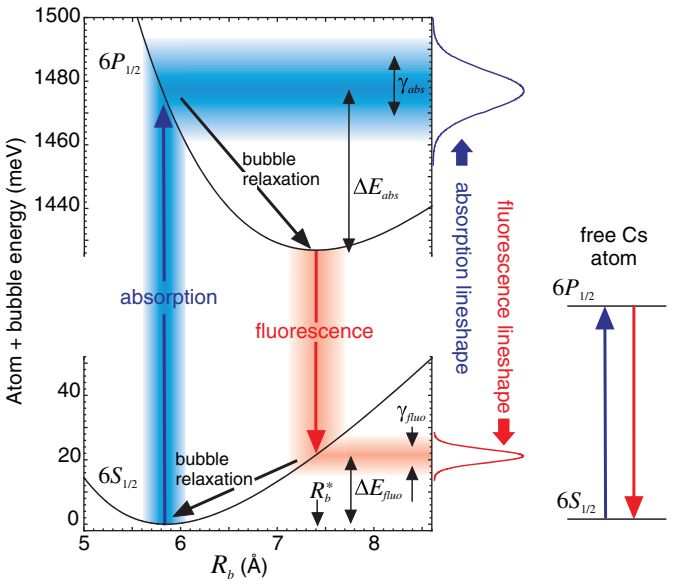

Fig. 1: (Color online) Potential energies as a function of the bubble radius R_b of an atomic bubble formed around a Cs atom in condensed ^{4}He [12,13]. Electronic transitions for absorption and fluorescence emission are represented as blue and red vertical arrows, respectively. The shaded bands show the delocalization of the bubble interface and the corresponding spectral-line broadening.

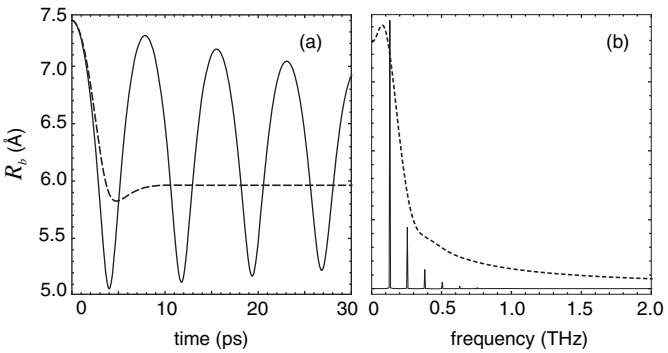

Fig. 2: Calculated dynamics of the bubble interface following fluorescence emission (a) and its Fourier spectrum (b). Cs atom in superfluid He at $T = 1.5\,\mathrm{K}$, $p_{\mathrm{stat}} = 20\,\mathrm{bar}$. Solid lines: solution of the Rayleigh-Plesset equation for incompressible liquid; dashed lines: solution of eq. (2). The initial bubble size, R_b^*, corresponds to the excited $6P_{1/2}$ state of the Cs atom in superfluid He.

the strong delocalization of the He atoms in the liquid and solid phases, one can treat condensed He as a continuous medium to which a hydrostatic model can be applied.

The total energy of the atom-plus-bubble system can be calculated as [12]

$$E_{\mathrm{tot}} = V_{\mathrm{int}} + p_{\mathrm{stat}} V_{\mathrm{bub}} + \sigma S_{\mathrm{bub}} + E_{\mathrm{vk}}, \qquad (1)$$

where p_{stat} and σ are the hydrostatic pressure and the surface tension parameter of liquid helium, $V_{\mathrm{bub}} \propto R_b^3$ and $S_{\mathrm{bub}} \propto R_b^2$ are the bubble volume and surface area, V_{int} is the impurity-helium interaction energy, and E_{vk} is a volume kinetic energy arising from the localization of the He atoms at the bubble interface. The atomic-bubble energetics are illustrated in fig. 1 by a potential diagram derived in [13] for a Cs atom in condensed He. The bubble shape and size are determined by the dopant's electron density distribution that differs significantly for the excited and ground states. The electronic transitions in the dopant occur in a fixed bubble configuration, $R_b = \mathrm{const}$, (Franck-Condon principle). Photon absorption occurs in the smaller bubble ($R_b = 5.8\,\mathrm{Å}$) formed by the ground state and is followed by a bubble expansion, while fluorescence emission occurs in a larger bubble ($R_b^* = 7.4\,\mathrm{Å}$) and is followed by the bubble contracting to its original size. In both processes the excess energy $\Delta E_{\mathrm{abs/fluo}}$ released during the bubble relaxation is transferred to the matrix.

Despite the small bubble size, this hydrostatic model successfully describes the experimentally observed spectroscopic properties of metallic dopants in liquid and solid helium (for a review see [11]). Here, we apply the same approach for investigating the atomic-bubble dynamics and solve numerically the nonlinear equation of motion

$$\left(1 - \frac{\dot{R}_b}{v_s}\right) R_b \ddot{R}_b + \frac{3}{2}\left(1 - \frac{\dot{R}_b}{3v_s}\right) \dot{R}_b^2 + \frac{4\mu}{\rho_0}\left(\frac{\dot{R}_b}{R_b} + \frac{\ddot{R}_b}{v_s}\right) + \frac{2\sigma}{\rho_0}\frac{1}{R_b} = \frac{p_a - p_{\mathrm{stat}}}{\rho_0} + \frac{\dot{R}_b R_b}{\rho_0 v_s}\frac{\mathrm{d}p_a}{\mathrm{d}R_b}, \qquad (2)$$

of the bubble interface, derived in [14]. Here ρ_0 and μ are the density and viscosity of the liquid, v_s is the sound velocity, and

$$p_a(R_b) = \frac{1}{S_{\mathrm{bub}}}\frac{\mathrm{d}V_{\mathrm{int}}}{\mathrm{d}R_b} \qquad (3)$$

is the pressure at the bubble interface due to the impurity-helium interaction.

In the limit of an infinitely large sound velocity ($v_s \to \infty$), eq. (2) reduces to the classical Rayleigh-Plesset equation for incompressible liquids. In fig. 2(a) we plot the dynamics of the atomic bubble formed by a Cs atom in superfluid helium at $T = 1.5\,\mathrm{K}$, $p_{\mathrm{stat}} = 20\,\mathrm{bar}$, calculated in this limit. The $p_a(R_b)$-dependence is derived from the potential curves of fig. 1. The initial bubble configuration corresponds to the excited $6P_{1/2}$ state of the Cs atom. The sudden change of p_a induced by the atomic fluorescence transition excites free bubble interface oscillations at the frequency ω_b. The only dissipation mechanism is due to the viscosity of the liquid that is very small in condensed helium [15]. In superfluid ^{4}He at 1.5 K, in the pressure range of 0–25 bar, the normal fluid fraction varies between 11% and 30% and has a viscosity of ≈ 15 micropoise. It leads to a damping time of 70–130 ps (fig. 2(a)). In normal-fluid He the viscosity is much larger (50–100 micropoise) and leads to a damping on the scale of several ps.

The Fourier-spectrum of the bubble oscillation is shown in fig. 2(b). It has a sharp fundamental component at

$\omega_b/2\pi \approx 0.15\,\mathrm{THz}$ ($\hbar\omega_b \approx 0.64\,\mathrm{meV}$) and overtones arising from the strong anharmonicity of the oscillations. Calculations in [12,13,16,17] assuming the $v_s \to \infty$ limit for different impurity atoms and He densities yield ω_b values in the range of 0.1–0.5 THz (0.4–2.2 meV), which overlaps with the spectrum of elementary excitations of condensed He. One therefore expects a strong resonant coupling between bubble vibrations and phonons.

An important aspect of this resonance is the relationship between the bubble size and the resonant phonons' wavelength. For the relatively large bubbles ($R_b > 1\,\mu\mathrm{m}$) studied so far in connection with underwater explosions, cavitation, and sonoluminescence (reviewed in [18]), the characteristic frequencies lie in the kHz range and the resonant sound waves have a wavelength $\lambda \gg R_b$. On the other hand, the nanometer-sized atomic bubbles studied here vibrate at THz frequencies and can thus excite phonons whose wavelength is on the order of several nanometers, *i.e.*, $\lambda \approx R_b$.

The coupling between bubble vibrations and phonons was addressed in early work on electron bubbles in superfluid helium [19,20]. Resonances between bubble vibration modes (breathing, dipole, etc.) and phonons should manifest themselves as peaks in the bubble-phonon scattering cross-section $A(k)$. For the electron bubble in ^{4}He ($R_b \approx 18\,$Å at satutated vapor pressure), the characteristic vibration frequencies $\omega_b \simeq 0.01\,\mathrm{THz}$ [19] are too small to be resolved spectroscopically. Only the integral cross-section A can be accessed by measurements of the electron mobility in a static electric field that is limited by collisions with thermal phonons [20]. However, the frequencies of the smaller *atomic* bubbles are significantly higher and can be studied by laser spectroscopy, as shown below.

Taking the finite compressibility of the liquid into account leads to a damping of the bubble oscillations due to the emission of sound waves. The efficiency of the damping strongly depends on the bubble size, *i.e.*, on the relationship between R_b and the sound wavelength λ. For the vibrations of macroscopically large bubbles, sound emission represents a minor decay channel as compared to viscous damping. However, for atomic bubbles in liquid helium (v_s around 300 m/s) this damping is much faster than the one due to viscosity, both in the superfluid and in the normal fluid phase. As shown in fig. 2, the oscillations become damped within a single period and their Fourier spectrum is very broad. A similar strong damping was observed in a recent experimental time-resolved study [21] of the larger bubbles ($R_b \approx 13$Å) formed by He_2^* excimers in superfluid helium.

The vibrating atomic bubble generates a set of matrix excitations whose frequencies ω_i and wave vectors $\vec{k_i}$ obey $\sum \hbar\omega_i = \Delta E_{\mathrm{abs/fluo}}$ and $\sum \vec{k_i} = 0$ (no center-of-mass motion). Depending on the amplitude of the bubble vibrations, we distinguish between *quasiclassical* wave packets and *quantum* wave packets that contain a very large or a very small number of phonons, respectively.

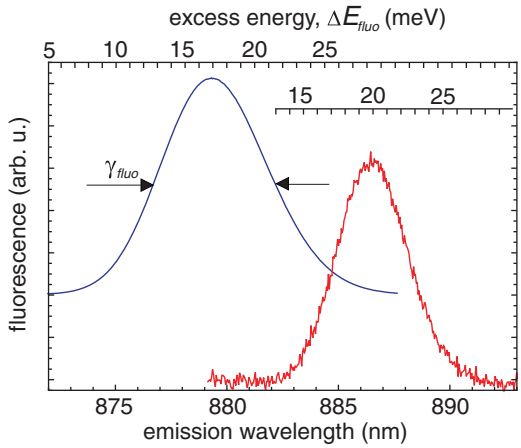

Fig. 3: (Color online) Fluorescence spectrum of the $6^2P_{1/2}$-$6^2S_{1/2}$ transition of Cs atoms in condensed He at $T = 1.5\,\mathrm{K}$. Upper curve: solid He at $p = 29\,\mathrm{bar}$; lower curve: superfluid He at $p = 20\,\mathrm{bar}$. The origin of the ΔE_{fluo} scale is calculated as discussed in [13] and differs for the two spectra.

The bubble formed by the Cs atom considered above exhibits quasiclassical behavior. As shown in fig. 1, the excess energy, $\Delta E_{\mathrm{fluo}} \approx 20\,\mathrm{meV}$ is much larger than $\hbar\omega_b$. The bubble is thus excited into a superposition of many vibration states. The discrete quantum nature of the oscillation modes will give the fluorescence spectrum a quasiperiodic structure, similar to the vibronic spectra of diatomic molecules. However, sound emission overdamps the oscillation and broadens each vibration mode to $\Gamma \geqslant \omega_b$, so that the adjacent vibrational lines in the fluorescence spectrum overlap, thereby completely smearing out their discrete structure. The smooth experimentally observed fluorescence spectrum of Cs in superfluid He shown in fig. 3 reflects this consideration. It has a structureless, nearly Gaussian lineshape with a spectral width $\gamma_{\mathrm{fluo}} \approx 10 \times \omega_b$. Most atomic dopants in condensed He and other rare-gas matrices studied up to date (see review in [11]) have similar broad absorption and fluorescence spectra without vibration substructure and thus belong to the same type.

The quantum regime of the dopant-phonon interaction is expected to occur for atomic transitions after which the bubble size relaxation produces a very small excess energy $\Delta E_{\mathrm{exci/fluo}}$ (fig. 1), such that only a few phonons are produced by a single atomic transition. One easily sees from fig. 1 that this happens when the minima of the excited- and ground-state potential curves lie at the same bubble radius. This condition is fulfilled by inner-shell transitions in impurity atoms which are screened from interactions with the surrounding matrix by outer valence electrons that leave the bubble configuration practically unperturbed [22–24].

In the quantum regime, transitions between the vibrational ground states of the lower and upper electronic states produce no phonons and their fluorescence spectrum consists of a sharp peak (zero-phonon line, ZPL) close

to the free atom's wavelength [25]. Transitions towards excited vibrational states create several phonons, thus leading to a broader spectral feature (phonon wing, PW) that is redshifted with respect to the free atomic line. ZPL and PW structures have been observed in the inner-shell spectra of the rare-earth elements Eu and Tm in liquid and solid helium [22,23], as well as in the spectra of molecules attached to helium nanodroplets [6,7].

The analysis above shows that the fluorescence spectrum emitted by an atom in a bubble provides information about the spectrum and amplitude of the generated phonon wave packet. In the quasiclassical regime, the number of generated phonons is not well defined and the spectrum of fig. 3 thus does not allow one to study bubble dynamics and its coupling to elementary excitations. In the quantum regime, on the other hand, the spectral profile of the phonon wing is a direct measure of the probability to excite a phonon with a given energy.

In order to study the bubble-phonon coupling quantitatively, we have carried out a new spectroscopic study of the transition metal atoms Au and Cu in condensed He, focussing on transitions involving $3d$ or $5d$ electrons that are screened by the outer $4s$ or $6s$ electrons for Cu or Au, respectively. We have observed the $5d^9 6s^2\ ^2D_{3/2}$-$5d^9 6s^2\ ^2D_{5/2}$ and $5d^9 6s^2\ ^2D_{3/2}$-$5d^{10} 6s\ ^2S_{1/2}$ fluorescence lines of Au and the $3d^9 4s^2\ ^2D_{3/2,5/2}$-$3d^{10} 4s\ ^2S_{1/2}$ lines of Cu. All four lines are forbidden in the free atom but can be observed in condensed-He matrices [24].

Our experimental setup is discussed in detail in [11]. A helium host matrix is doped with Au (Cu) atoms by means of laser ablation with the second harmonic of a pulsed Nd:YAG laser (532 nm, 50 mJ/pulse) focused onto a solid metal target. Measurements were performed in superfluid, normal fluid, and hcp (hexagonal close-packed) solid ^{4}He, in the pressure range of 7–30 bar, at 1.5 and 2.2 K. The Au (Cu) atoms isolated in the helium matrix are excited by the third harmonic of a second Nd:YAG laser (355 nm, 20 mJ/pulse) and their laser-induced fluorescence is analyzed by a grating spectrograph equipped with a CCD camera.

A typical fluorescence spectrum of the $^2D_{3/2}$-$^2D_{5/2}$ line of Au in *solid* ^{4}He (fig. 4(a)) shows clearly the ZPL and PW features (note the reduced scale of the ZPL on the left in (a)).

The relative contribution to the total intensity from N-phonon processes is given [25] by

$$P_N = S^N e^{-S}/N!, \qquad (4)$$

where S is the Huang-Rhys factor that is related to the relative intensity of the ZPL via $S = -\ln(I_{\rm ZPL}/I_{\rm tot})$. For the data of fig. 4 $S \approx 0.1$. The PW spectrum is thus dominated by the lowest-order processes. The only $N = 1$ process that satisfies the condition $\sum \vec{k}_i = 0$ involves the $k = 0$ optical phonon whose energy is known from inelastic neutron and Raman scattering to be $\hbar\omega_{\rm optic} \approx 1$ meV [5,26]. However, our experimental PW spectra contain no features that can be associated with this process.

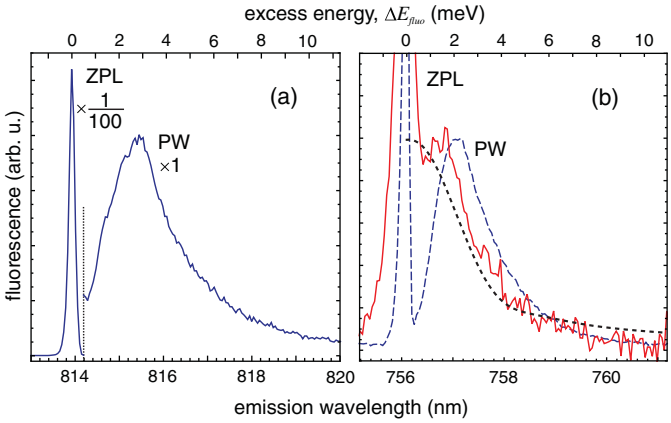

Fig. 4: (Color online) Fluorescence spectra of the forbidden inner-shell transitions of Au and Cu in condensed He. (a) $^2D_{3/2}$-$^2D_{5/2}$ line of Au in solid He at $T = 1.5$ K, $p = 30$ bar; (b) $^2D_{3/2}$-$^2S_{1/2}$ line of Cu in solid He at 1.5 K and 30 bar (dashed line) and in normal fluid He at 2.2 K and 16 bar (solid line). The spectrum of the calculated bubble dynamics is shown in (b) as dotted curve.

An optical phonon corresponds to two neighboring He atoms within the same elementary cell ($d = 3.67$ Å [26]) that oscillate against each other. The coupling of this mode to the expansion/contraction of a bubble with a typical diameter of 8–15 Å is expected to be very weak. We therefore conclude that the observed PW spectrum is due to $N = 2$ processes. The PW lineshape is indeed very similar to the one recorded by two-phonon Raman scattering [5]. The PW intensity at $\Delta E_{\rm fluo} = 2\hbar\omega$ is thus proportional to the probability $W(\omega)$ for generating a phonon pair with frequency ω.

The PW contours of the three fluorescence lines $^2D_{3/2,5/2}$-$^2S_{1/2}$ studied in *solid* ^{4}He (fig. 4(b)) are very similar to the one shown in fig. 4(a). These lines correspond to transitions between the inner $(n-1)d$ and the outer ns shells which are more strongly coupled to the helium environment than the $^2D_{3/2}$-$^2D_{5/2}$ transition within the $(n-1)d$ shell. Their Huang-Rhys factors, determined from the relative intensities of the PW and the ZPL lie in the range $S = 1.29$–1.39.

The fluorescence spectrum obtained in *liquid* He is also shown in fig 4(b). The lower fluorescence intensity in liquid He forced us to record the signals with a larger aperture of the spectrometer. As a consequence the reduced spectral resolution leads to a broadening of the ZPL. The PW spectrum in liquid He is narrower than in solid He and its maximum lies closer to the ZPL. Our observations thus suggest that the shape of the PW is a sensitive measure of matrix properties.

The wave packets formed by the emitted phonons can be modeled as a superposition

$$\Psi(r,t) = \int W(\omega) j_0(kr) e^{i\omega t} {\rm d}\omega \qquad (5)$$

of isotropic classical sound waves that propagate radially outward from the bubble. $W(\omega)$ corresponds to the PW

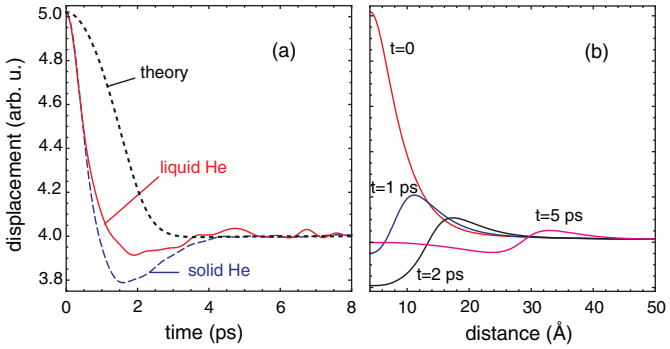

Fig. 5: (Color online) Wave packet created by a vibrating atomic bubble formed by a Cu atom in condensed He. (a) Motion of the atomic-bubble boundary in liquid (solid line) and in solid (dashed line) He. The dotted line shows the calculated time-dependent bubble radius $R_b(t)$ for liquid He. (b) Atomic displacements in solid He as a function of the distance from the bubble center at $t = 0$, 1, 2, and 5 ps.

lineshape and $j_0(kr)$ is a spherical Bessel function. We have applied this model to the data of fig. 4(b) corresponding to pressurized normal fluid and solid helium. We assume a linear dependence $k(\omega)$ that is, strictly speaking, valid only for small ω. For liquid He the slope is determined by the sound velocity ($v_s = 320\,\mathrm{m/s}$ at $T = 2.2\,\mathrm{K}$, $p = 16\,\mathrm{bar}$). For solid He it is chosen to be $v_s = 500\,\mathrm{m/s}$ in order to satisfy approximately the dispersion relation $k(\omega)$ for longitudinal acoustic phonons [26], neglecting its anisotropy. The sound waves with different frequencies are synchronized at the onset ($t = 0$) of fluorescence emission and then quickly dephase, leaving the bubble in a new equilibrium configuration. The resulting motion of the bubble interface is shown in fig. 5(a). The bubble undergoes a very fast contraction that is followed by a much slower expansion that reaches an equilibrium value at $t \approx 5\,\mathrm{ps}$. The dynamics in the solid phase is very similar to that in liquid, with a more pronounced undershot at $t \approx 1.5\,\mathrm{ps}$.

In fig. 5(b) we plot snapshots of the displacements of He atoms in the vicinity of the bubble at $t = 0$, 1, 2, and 5 ps. As the wave packet moves away from the bubble its amplitude decreases as $1/r$; therefore, only atoms at $r \leqslant 50\,\text{Å}$ experience a significant displacement.

In fig. 5(a) we also show $R_b(t)$ obtained by a numerical solution of eq. (2) for the Cu atom in liquid He (dotted curve). The corresponding $p_a(R_b)$ is calculated using the Cu-He pair potential from [27]. The ground-state atomic bubble has a radius of 4.0 Å that is significantly smaller than R_b for Cs. In this case the phonon coupling is even stronger and the bubble does not vibrate at all. The bubble contraction time is $\approx 2\,\mathrm{ps}$, very close to the value inferred from the experimental PW data. The Fourier spectrum of the calculated $R_b(t)$ is shown in fig. 4(b) and is in a good agreement with the experimental PW contour in liquid He.

The initial phase of the calculated dynamics is significantly slower than that inferred from the experimental spectra. We attribute this discrepancy to variations of the bubble interface thickness that are not reproduced by eq. (2). The helium density profile $\rho(r)$ at the bubble interface is described [13] by a smooth function, such that $\rho(r) = 0$ inside the bubble and $\rho(r) = \rho_0$ outside. As shown in [9,10], the *expansion* of the bubble starts as an increase of the steepness of the interfacial function $\rho(r)$ that is followed by a much slower breathing oscillation. This surface mode is expected to contribute also to the bubble *contraction* process studied here.

In summary we have shown that the fluorescence emission by an impurity atom in condensed He creates a strongly localized wave packet of matrix phonons. The parameters of this wave packet can be derived from experimental fluorescence lineshapes and agree well with the prediction from a hydrodynamic bubble model.

* * *

This work was supported by grant No. 200020-129831 of the Schweizerischer Nationalfonds. We acknowledge stimulating discussions with D. Baeriswyl and J. P. Toennies.

REFERENCES

[1] Landau L., *Phys. Rev.*, **60** (1941) 356.
[2] Clements B. E., Godfrin H., Krotscheck E., Lauter H. J., Leiderer P., Passiouk V. and Timczak C. J., *Phys. Rev. B*, **53** (1996) 12242.
[3] Bossy J., Pearce J. V., Schober H. and Glyde H. R., *Phys. Rev. B*, **78** (2008) 224507.
[4] Blackburn E., Goodkind J., Sinha S. K., Broholm C., Copley J. and Erwin R., *Pramana - J. Phys.*, **71** (2008) 673.
[5] Surko C. M. and Slusher R. E., *Phys. Rev. B*, **13** (1976) 1095.
[6] Hartmann M., Mielke F., Toennies J. P., Vilesov A. F. and Benedek G., *Phys. Rev. Lett.*, **76** (1996) 4560.
[7] Toennies J. P. and Vilesov A. F., *Angew. Chem., Int. Ed.*, **43** (2004) 2622.
[8] Huang P. and Whaley K. B., *Phys. Rev. B*, **67** (2003) 155419.
[9] Eloranta J. and Apkarian V. A., *J. Chem. Phys.*, **117** (2002) 10139.
[10] Eloranta J., Seferyan H. Y. and Apkarian V. A., *Chem. Phys. Lett.*, **396** (2004) 155.
[11] Moroshkin P., Hofer A. and Weis A., *Phys. Rep.*, **469** (2008) 1.
[12] Kinoshita T., Fukuda K., Takahashi Y. and Yabuzaki T., *Phys. Rev. A*, **52** (1995) 2707.
[13] Hofer A., Moroshkin P., Ulzega S., Nettels D., Müller-Siebert R. and Weis A., *Phys. Rev. A*, **76** (2007) 022502.
[14] Keller J. B. and Miksis M., *J. Acoust. Soc. Am.*, **68** (1980) 628.

[15] Wilks J., *The Properties of Liquid and Solid Helium* (Clarendon Press) 1967.
[16] Bauer H., Beau M., Friedl B., Marchand C., Miltner K. and Reyher H. J., *Phys. Lett. A*, **146** (1990) 134.
[17] Moriwaki Y. and Morita N., *Eur. Phys. J. D*, **13** (2001) 11.
[18] Lauterborn W. and Kurz T., *Rep. Prog. Phys.*, **73** (2010) 106501.
[19] Celli V., Cohen M. H. and Zuckerman M. J., *Phys. Rev.*, **173** (1968) 253.
[20] Baym G., Barrera R. G. and Pethick C. J., *Phys. Rev. Lett.*, **22** (1969) 20.
[21] Benderskii A. V., Eloranta J., Zadoyan R. and Apkarian V. A., *J. Chem. Phys.*, **117** (2002) 1201.
[22] Hui Q. and Takami M., *J. Low Temp. Phys.*, **119** (2000) 393.
[23] Ishikawa K., Hatakeyama A., Gosyono-o K., Wada S., Takahashi Y. and Yabuzaki T., *Phys. Rev. B*, **56** (1997) 780.
[24] Moroshkin P., Lebedev V. and Weis A., *J. Low Temp. Phys.*, **162** (2011) 710.
[25] Pryce M. H. L., in *Phonons in Perfect Lattices and in Lattices with Point Imperfections*, edited by Stevenson R. W. H. (Oliver and Boyd) 1966, p. 403.
[26] Minkiewicz V. J., Kitchens T. A., Lipschultz F. P., Nathans R. and Shirane G., *Phys. Rev.*, **174** (1968) 267.
[27] Cargnoni F., Kus T., Mella M. and Bartlett R. J., *J. Chem. Phys.*, **129** (2008) 204307.